

# Comparison of PIV and SPIV in Application to Industrial Spray Burner

Virginia Palero, Yuji Ikeda, Tsuyoshi Nakajima

Kobe University

Rokkodai, Nada, Kobe 657-8501 JAPAN

Joseph Shakal

TSI Inc. Laser Diagnostics Division,

St Paul, Minnesota, USA

## ABSTRACT

The purpose of this paper is to investigate and evaluate Stereoscopic PIV (SPIV) in spray measurements. The system studied here is a gun-type burner (figure 1) used for practical industrial oil furnaces of 0.1 MW and spray measurement is done under no reacting condition. The SPIV angular displacement method has been implemented. Several parametric studies have been done in order to optimize the most suitable stereoscopic angle for our particular set-up (22.5°) and also to estimate SPIV accuracy.

SPIV has been compared with PDA (SMD and size-classified PDA) showing good agreement specially between SPIV data and PDA velocities obtained for particles smaller than 30  $\mu\text{m}$ . Figure 2 shows the swirl component contours obtained with both techniques.

In-plane velocity components obtained with PIV are affected by an error because of the out-of-plane component. Therefore, SPIV will provide, not only the out-of-plane component, but also will correct the in-plane components. In this paper SPIV has been compared also with PIV in order to determine the magnitude of this correction. SPIV corrects the in-plane velocity components in a 10% of the maximum measured velocity.

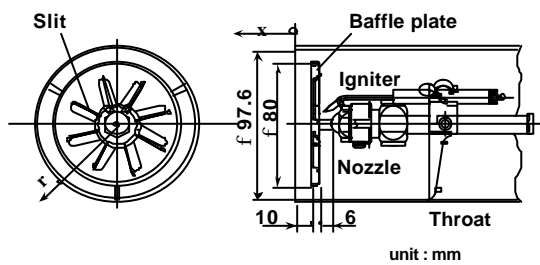


Figure 1 Gun-type burner

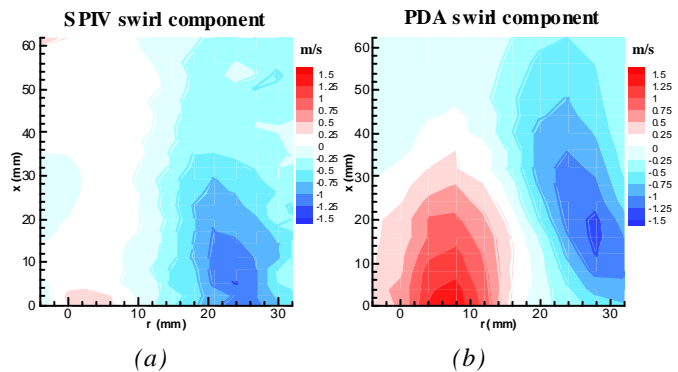


Figure 2 Swirl component contours obtained by: (a) SPIV, (b) PDA

## 1. INTRODUCTION

Laser measurement techniques for flow analysis have been developed to understand flow structures and their temporal and spatial characteristics. Laser Doppler Velocimetry (LDV) and Phase Doppler Anemometry (PDA), as point techniques, describe turbulent characteristics and droplet dynamics at very high data rates, but it is hard to gain insight about spatial structures in the flow.

Particle Image Velocimetry is a well-known measurement technique for the in-plane velocity components in a whole fluid plane (Grant 1997, Raffel et al., 1998). But it has some limitations, such as time series data, turbulent spectrum analysis or small spatial resolution. Moreover, it is clear that PIV includes information from many different particle sizes that happen to be in the measurement plane, and the particle number density is one of the major error sources in PIV measurement. Furthermore, if the flow is three dimensional, the out-of-plane component is a source of error in the measured in-plane components (Prasad and Adrian, 1993). The measured components have an additional term, that is proportional to the out-of-plane component and that increases as the measurement point is far from the camera axis. In spite of these disadvantages, PIV has been implemented in many different applications and has demonstrated its special ability to make full field flow measurements.

Recently, some efforts have been made to extend PIV to the measurement of whole three-dimensional velocity fields. The most straightforward approach is based on stereoscopic viewing of the fluid plane, with the translational and angular displacement methods being the most popular configurations (Gauthier and Riethmuller, 1988). In the translational method, the optical axis of the cameras are parallel to each other and perpendicular to the fluid plane (Arroyo and Greated, 1991, Palero et al., 2000) while in the angular method the camera axis forms a certain angle (called stereoscopic angle) with the fluid plane's normal (Prasad and Adrian, 1993, Prasad and Jensen, 1995). Stereoscopic PIV (SPIV) can not only provide the whole velocity vector but also give the in-plane components without the error due to the perspective.

In our previous works the spray characteristics of a gun-type burner have been measured and discussed (Ikeda et al., 1995, Kawahara et al., 1996, 1997). Figure 1 shows the gun-type burner used in these studies. This type of oil burner is commercially available for rather small (0.1 MW class) industrial furnaces and boilers. The baffle plate serves as a flame holder and aids in reducing soot formation. The heavy oil (type A, Japanese Industrial Standard) was pressurized up to 0.7 MPa and a hollow cone spray was produced with a  $60^\circ$  included angle.

Figure 2 shows a direct picture of the flame used in these measurements (Ikeda et al., 1995). There are three main regions: one is the flame-holding region near the baffle plate, the second is the transparent region where the fuel droplets are evaporating, and the last one is the main combustion region containing much soot luminescence.

Initial experiments were done by PDA, and droplet behavior was described by size-classified PDA measurements (Kawahara et al., 1997). Under both, isothermal and reacting conditions, it was found that droplets under  $30\ \mu\text{m}$  in diameter could follow the reversing flow at the flame-holding region, and droplets over  $50\ \mu\text{m}$  in diameter penetrated the reversing flow.

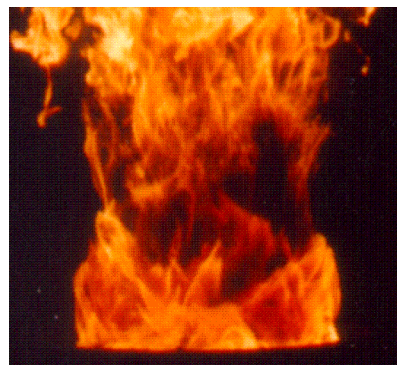
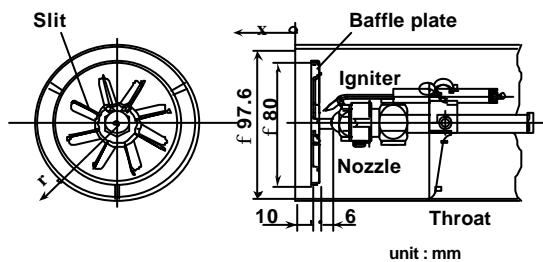


**Figure 1** Gun-type burner

**Figure 2** Direct flame image

However, since PDA can not provide information about flow and spray in terms of spatial structures, PIV arises as a suitable choice although it has some drawbacks that might prevent its general application to a spray (impossibility of distinguish different particle sizes or particle number densities, as mentioned before). Nevertheless, PIV has been applied in this spray in reacting and non-reacting conditions, and the results were compared with size-classified PDA (Ikeda et al., 1998, 1999). The results showed good agreement between PIV measurements and PDA-measured velocities of 20 to 30  $\mu\text{m}$  droplets.

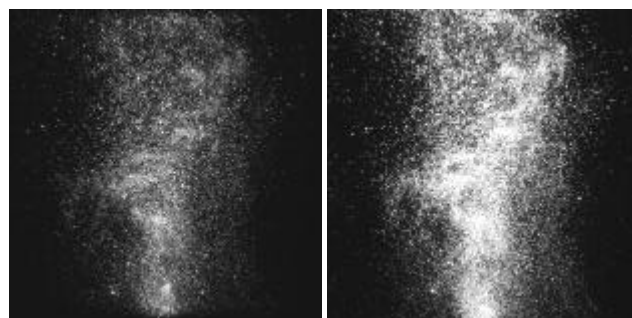
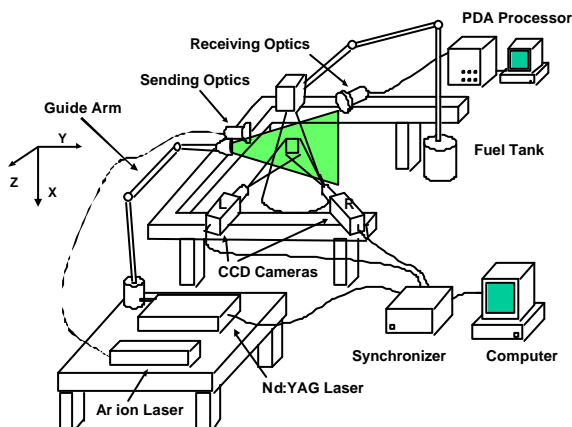
Much more work has to be done in order to optimize PIV application to sprays. First, further knowledge on droplet dynamics is needed. That implies the development of new techniques that will provide information about particle sizes. With this purpose Multi-Intensity Layer PIV is proposed as a technique for obtaining droplet size information by accounting for differences in scattered light intensity (Yamada et al, 1998). Second, PIV does not provide the three velocity components vector map. Therefore, any improvement of the measurements has to consider the measurement of the full velocity vector.

SPIV has been successfully applied to air flows (Arroyo and Greated, 1991, Willert, 1997) and to liquid flows (Prasad and Adrian, 1993, Prasad and Jensen, 1995, Palero et al., 2000) and in this paper SPIV (angular displacement method) will show its applicability to a gun-type burner in non-reacting condition. Here, four subjects will be investigated: problem understanding, PIV applicability to a spray, error estimation of PIV in spray with PDA data and discussion of industrial spray burner by SPIV data. Several parameters have to be optimized as laser sheet thickness, time separation between laser pulses, camera aperture and interrogation area. It is important to find the most dominant parameter to optimize SPIV set-up and examine spray measurements. This parameter optimization is beyond the scope of this paper but it has been accomplished in other work (Palero et al., 2000). Future work involves SPIV application under reacting condition as well as the implementation of the Multi-intensity technique in SPIV.

## 2- EXPERIMENTAL SET-UP

### 2.1. SPIV set-up

Figure 3 shows the experimental set-up used in this work. In particular the SPIV and PDA set-up are presented. For SPIV application, a dual-cavity Nd:YAG laser (SP PIV-400, 400 mJ pulse a 532 nm) formed a sheet 2 mm thick for illumination. Two CCD cameras (TSI PIVCAM 10-30, cross-correlation, 1000x1016 pixels, Kodak ES1.0) were used with a 60 mm focal length Micro Nikkor lenses. Figure 4 shows the typical images recorded with this SPIV set-up. Light intensities in the left and right images were different from each other, as the forward-scattered light was stronger. Due to the intensity difference between the two images, the laser power and camera aperture had to be carefully adjusted. Image saturation had to be avoided in the right image, and the light intensity had to be strong enough in the left image in order to minimize the number of bad vectors. In this case, both cameras were working at f/4 and laser power was adjusted until a reasonable image quality was obtained for both images simultaneously.



(a)

(b)

**Figure 3** Schematic diagram of experimental set-up **Figure 4** SPIV image pair (a) left camera; (b) right camera

Here, the stereoscopic angular displacement arrangement has been used. As known, in the angular displacement method the image plane is not parallel to the lens plane. In order to have the whole plane in focus we need to use high f#. A large depth of focus can be obtained but a smaller fraction of the light scattered by the particles will reach the CCD sensor. Therefore, stronger laser power is required. A second method to obtain images focused is to apply the Scheimpflug condition, i.e., the object plane, the lens plane and the image plane have to intersect at a common line. Rotating the camera body or the lens to a certain angle accomplishes this. Thus lens can operate with the same aperture settings as in two-dimensional PIV. The Scheimpflug camera arrangement introduces perspective distortion to the images, causing a rectangle in the light sheet plane to be imaged as a trapezoid on the image sensor. Obviously, the image magnification is not uniform.

A simple calibration factor for converting from the fluid to image planes can not be used. In order to map points in the fluid to image location properly, a more complex mapping function is needed, normally a set of polynomial equations (Willert, 1997). To measure and correct the perspective distortion, a calibration procedure is used. The calibration target was chromed glass with a grid of 13x11, 200 μm diameter holes on 5 mm centers. The target was backlit with the holes acting as light sources. Five images were recorded while moving this object 0.25 mm in the OZ direction. Using this grid of points, a set of third order calibration equations was computed for each axis (Bjorkquist, 1998).

A PC with two frame-grabbers acquired and processed the images. 450 stereoscopic image pairs were recorded in 45s then transferred from RAM to the hard disk. These images were analyzed using the Insight software (ver 3.00 TSI Inc) using the cross-correlated subregions of frame-straddle images.

SPIV accuracy is affected by the elimination of spurious vectors and the interpolation of the “holes”, which arise when a good correlation is not obtained in the processing of the two stereoscopic images. Spurious vectors in the two dimensional maps are eliminated using, first, a range filter (the vector can not exceed reasonable limits in the U and V displacement) and, second, the vector value has to be similar to the mean value of the nearest neighboring vectors (Keane and Adrian, 1990). 3D vector maps are computed by interpolating the two 2D vector fields in a new grid created to define the locations where the three-dimensional velocity is desired. For the best results the number of three-dimensional vectors should be about as the same as the number of two-dimensional vectors.

## **2.2 SPIV optimization**

To analyze the performance and the accuracy of the stereoscopic system, several test have been done by controlled displacement an object. The object (black dots printed on a white paper) was mounted on a system that allowed its rotation and translation and was illuminated with white light. The first experiment was directed to determine the optimum stereoscopic angle ( $\alpha$ ) in our particular set-up. Lawson and Wu (1997), suggested the optimum stereoscopic angle to be  $20^\circ < \alpha < 30^\circ$  as a way to compensate for the rms error in the out-of-plane component (which decreases when  $\alpha$  increases) and the rms in the in-plane components (which increases with  $\alpha$ ). Following this criterion, four stereoscopic angles have been tested (20°, 22.5°, 25° and 30°). The object was rotated in the XZ plane (0.5°, 1°, 1.5°, 2°, and 2.5°) in order to have different displacement in the OZ direction across the plane.

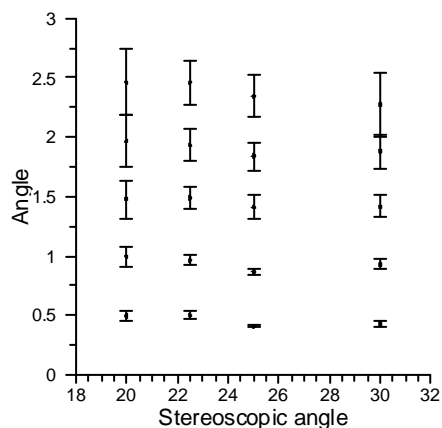


**Figure 5** Displacement angles measured at different stereoscopic angles and its rms (900 samples).

The measured displacement as well as the rms are plotted in figure 5. The rms increases with the rotation angle (due to particle defocusing) and is larger for  $\alpha = 20^\circ$  and  $30^\circ$ . For a rotation angle of only  $0.5^\circ$  (maximum displacement 0.9 mm) all the stereoscopic angles provide small rms ( $0.077^\circ$  for  $\alpha = 20^\circ$  and  $0.021^\circ$  for  $\alpha = 25^\circ$ ). Rms values obtained for  $22.5^\circ$  and  $25^\circ$  are very similar, slightly smaller for  $25^\circ$ , although appears that some systematic error has been introduced for  $25^\circ$  since the measured angles are biased a constant quantity, giving smaller values than expected. Finally a stereoscopic angle of  $22.5^\circ$  has been chosen as the most suitable angle for our work ( $2\alpha = 45^\circ$ ). This choice is also related with the future experiments in combusting conditions (Ikeda et al., 1999), where the test rig allows a maximum  $22^\circ$  included angle between the cameras.

In the second experiment, with a fixed stereoscopic angle  $\alpha = 22.5^\circ$ , the test object was translated in different directions, with displacements ranging from  $50 \mu\text{m}$  up to  $1500 \mu\text{m}$  (along the OZ axis) and from  $100 \mu\text{m}$  up to  $500 \mu\text{m}$  (along radial (OY) direction). The maximum rms errors measured were 3.8% and 1.4% for the OZ and OX displacement respectively, both obtained with the smaller displacements.

### 2.3 PDA set-up

For the PDA measurements a Dantec Phase Doppler Velocimeter was used. The dual beam system was comprised a 5W (nominal power)  $\text{Ar}^+$  laser and a conventional fiber optic PDA transmitter with a 40 MHz Bragg cell for frequency shifting and a 500 mm focal length front lens. The diameter of the geometrical probe volume was 0.1 mm and its length 1 mm. A Dantec PDA processor, with  $1 \mu\text{s}$  time resolution, was used for data acquisition.

## 3. RESULTS AND DISCUSSION

### 3.1 SPIV vs PDA

For the SPIV and PDA comparison the measuring area in the flow was  $72 \times 66 \text{ mm}^2$  (spatial resolution of 13.9 pixels/mm in the radial (OY) direction and 15.4 pixels/mm in the axial (OX) direction). The PDA system was set up to measure the axial and swirl components. PDA measurements (10.000 samples in each point) were done just after finishing the SPIV image acquisition (900 samples,  $20 \mu\text{s}$  pulse separation, laser thickness: 2 mm). For SPIV image analysis, grid spacing in the three-dimensional map was 2 mm, that is  $36 \times 33$  measured vectors, interpolated from  $60 \times 60$  vectors calculated in each stereoscopic image (50% overlap).

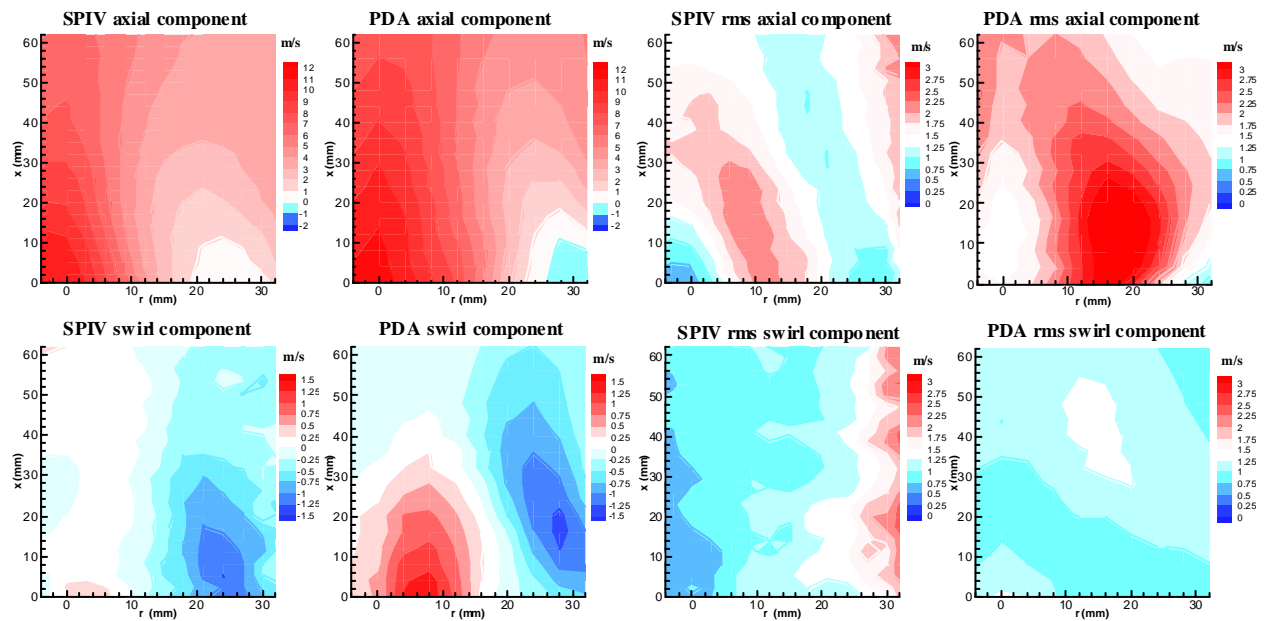


**Figure 6** SPIV vs PDA: axial and swirl components

Axial and swirl velocity contours are shown in figure 6. Near the burner axis droplets travel at high velocities (specially near the baffle plate ~12 m/s). There was a recirculation zone which size and location were not easy to measure in PIV, but clear in PDA, as can be seen from the differences between both contour maps. Between the center and this recirculation zone was a shear flow region, resulting from the gas flow-droplet interaction. The swirl component measured by both techniques indicates two regions where the flow was moving in opposite directions. The area with negative swirl component is measured accurately with both techniques, but there is important difference in the area with positive swirl values. With SPIV the mean swirl velocity in that area is about 0 m/s, while PDA values were about 1.5 m/s.

**Figure 7** SPIV and PDA rms contours.

In figure 7, rms contours are compared in order to quantify these two measurement techniques. These figures show high rms (axial) area from  $(x, r) = (45, 0)$  mm to  $(x, r) = (0, 15)$  mm. A higher turbulence intensity exists here because of the initial droplet angle, strong shear flow, large velocity gradient and air-droplet mixing. The swirl rms shows larger values on the right image edge. In that region the particle density was very low, in which increased the number of bad vectors with SPIV and decreased PDA data rate.

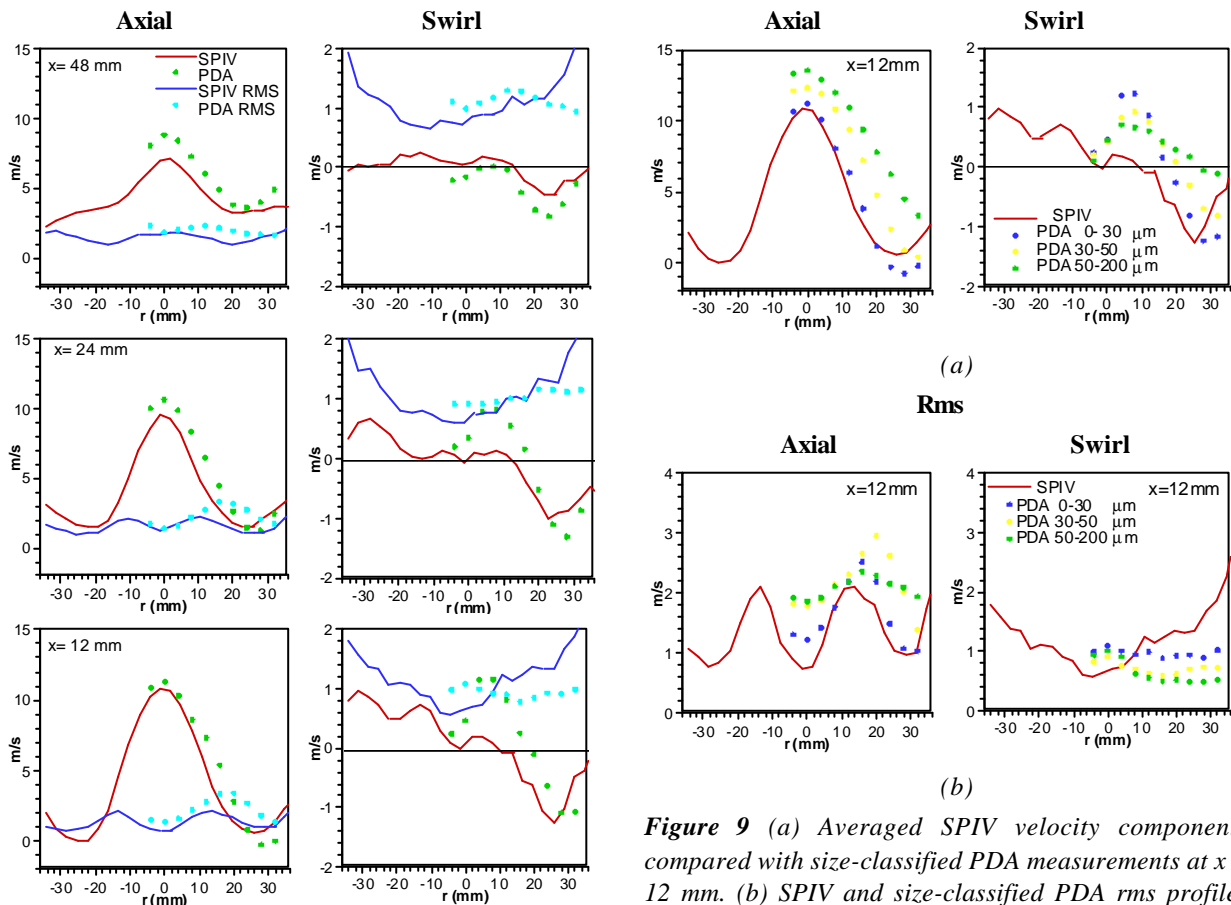


**Figure 8** Averaged velocity and rms measured by SPIV and PDA at  $x = 12, 24$  and  $48$  mm

**Figure 9** (a) Averaged SPIV velocity components compared with size-classified PDA measurements at  $x = 12$  mm. (b) SPIV and size-classified PDA rms profiles measured at  $x = 12$  mm.

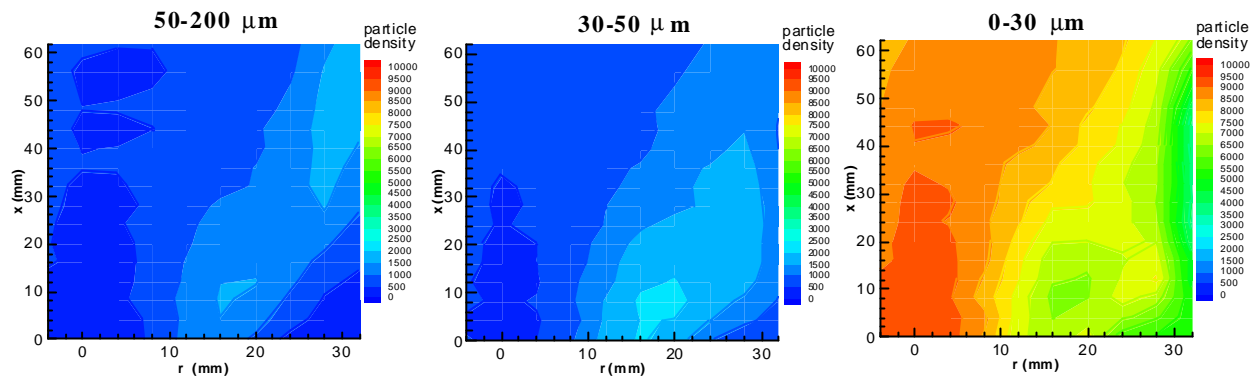


**Figure 10** Particle density distribution

Velocity components and rms are compared in detail at three different distances along the spray axis: 12, 24 and 48 mm (figure 8). PDA (SMD) data have a good agreement with the SPIV axial component. SPIV and PDA rms peaks are shifted and their height decreases upstream, indicating that the turbulence is decreasing far from the baffle plate. For the swirl component, PDA shows higher values near the spray axis than SPIV ( $x = 12, 24$  mm). But these differences almost disappear upstream.

A comparison between SPIV and size-classified PDA is shown in figure 9, for  $x = 12$  mm. Droplet sizes were classified in three layers:  $< 30 \mu\text{m}$ ,  $30$  to  $50 \mu\text{m}$  and  $> 50 \mu\text{m}$ . This particular classification is based on previous works (Kawahara et al., 1996) in which PDA measurements showed that particles bigger than  $50 \mu\text{m}$  penetrate the air flow while particles smaller than  $30 \mu\text{m}$  were entrained the recirculation zone where they played an essential role in flame holding for spray combustion. From these figures it is possible to see that the axial component measured by SPIV shows good agreement with sub- $30 \mu\text{m}$  PDA data. That is not surprising as in this spray most of droplets belong to this size range (figure 10). But also implies a loss of information about droplets with different sizes, pointing out the need of supplementary techniques for size discrimination in spray PIV. The swirl component also shows better agreement between SPIV and sub- $30 \mu\text{m}$  PDA particles. The velocity fluctuation is bigger for the smaller droplets, as they are more affected by the swirl motion, and has the same magnitude than the fluctuations obtained with SPIV.

### **3.2 SPIV vs PIV**

The experiments of SPIV and PIV were carried out using three CCD cameras, adding one more camera (we will call it camera M) between the two stereoscopic cameras (L and R) in figure 3 set-up (L= left camera, M = middle camera and R= right camera). It was not possible to record images simultaneously with the three cameras so images were recorded first using cameras L and M ( $2\alpha = 22.5^\circ$ ) and L and R ( $2\alpha = 45^\circ$ ). With the first configuration it is possible to have PIV and SPIV simultaneous measurements using M camera as a 2D PIV camera and as a part of the stereoscopic pair. The commune viewed area was  $72 \times 70 \text{ mm}^2$ .

In figure 11, comparisons were made in order to optimize SPIV set up and examine its application to practical spray burner. The averaged (900 samples) velocity vector maps and velocity components contours are shown. A pulse separation of  $20 \mu\text{s}$  and an interrogation area of  $32 \times 32$  were selected. The first column of graphics corresponds to the velocity obtained from camera M (PIV). The second column corresponds to the data extracted from cameras L and M (SPIV  $22.5^\circ$ ) and the last column to the data obtained form L and R (SPIV  $45^\circ$ ).

At the center axis, the axial velocities measured in the three cases were almost the same. The axial velocity decay along the axis is also the same. The reddest region of high axial velocity describes that there were fewer discrepancies in these three methods in terms of axial velocity measurement. The white region is showing the reversing flow area, which is playing the role of flame holding. Due to the location of the illuminated plane related to the baffle plate slits (figure 1) sizes of the two reversing flow regions differ from each other. On the right hand side, the air-flow was passing from the slit which pushed the reversing region downstream, while the left was not on the slit plane. Where

there is a slit, the flow through it causes positive axial velocity, so that the negative axial velocity decreased and weak reversing flow was produced.

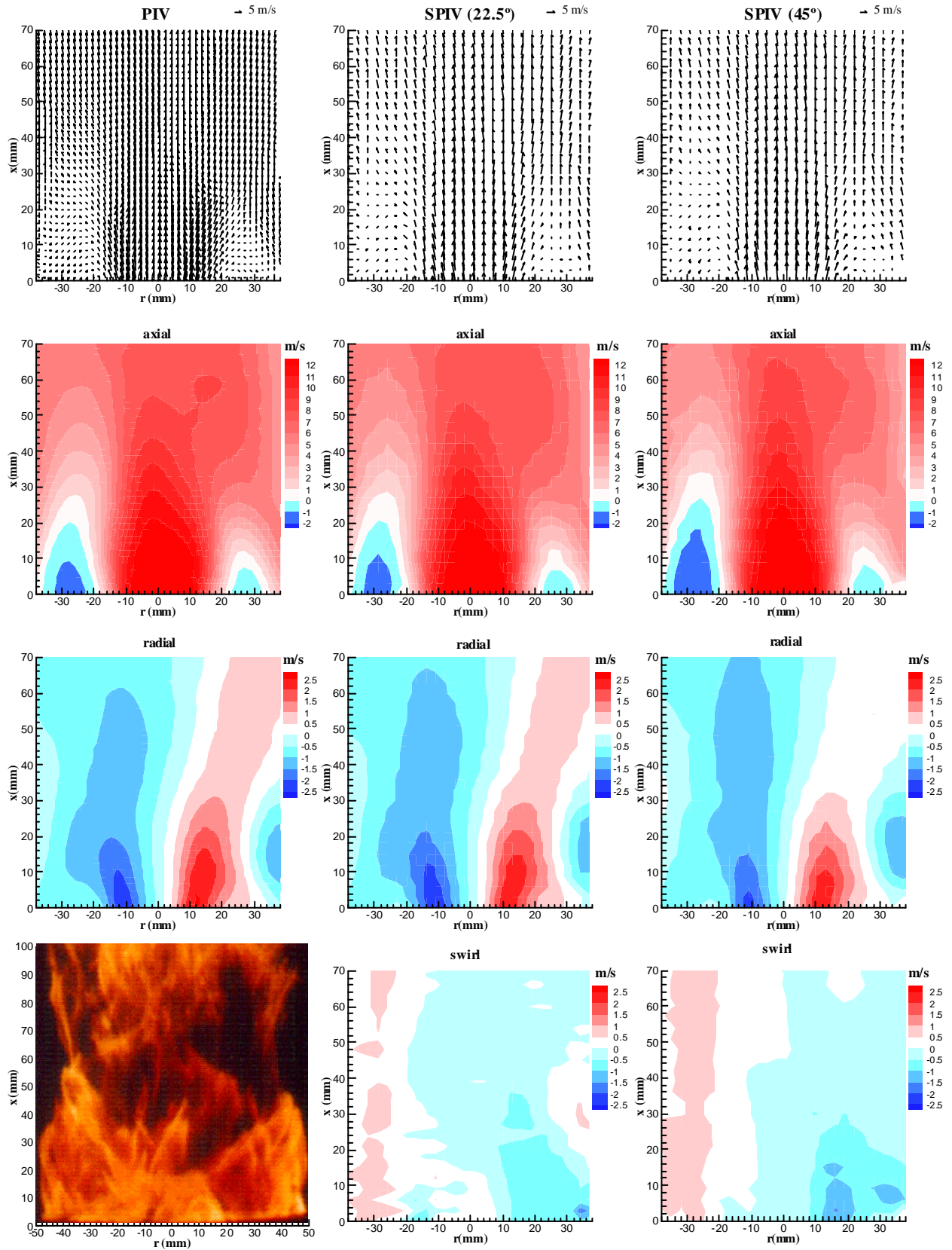




**Figure 11** Averaged velocity vectors maps (900 samples) obtained by PIV, SPIV ( $\alpha = 22.5^\circ$ ) and SPIV ( $\alpha = 45^\circ$ ) and averaged velocity components.

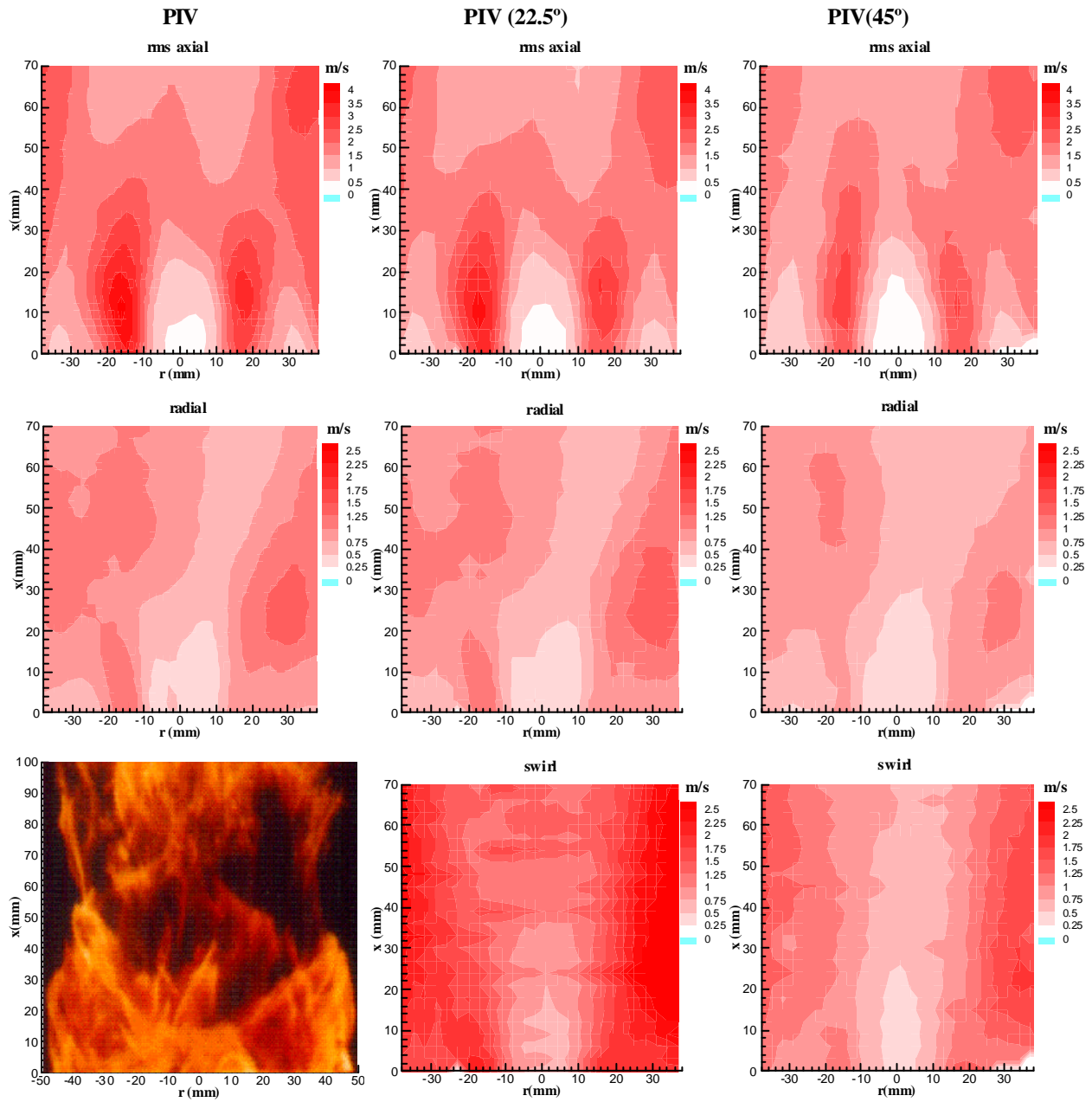


**Figure 12** Averaged rms contours (900 samples) obtained by PIV, SPIV ( $\alpha = 22.5^\circ$ ) and SPIV ( $\alpha = 45^\circ$ ) on each averaged velocity component.

PIV

SPIV ( $22.5^\circ$ )

SPIV ( $45^\circ$ )

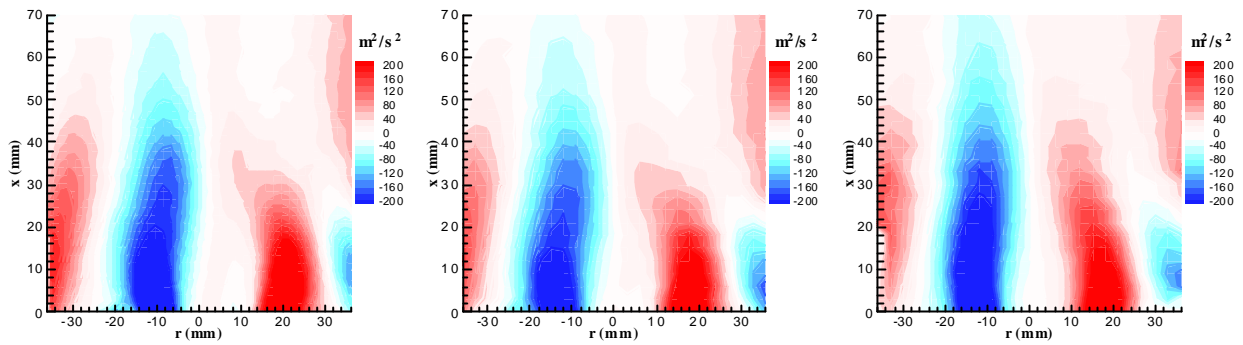


**Figure 13** Vorticity contours.

In radial velocity contours, it may say that SPIV (22.5°) shows better results than those obtained for SPIV (45°). The size and location of flow entrainment from outer side agrees with PIV. Furthermore, positive radial velocity was observed even downstream in SPIV (22.5°) and can represent the spray flow characteristics well. On the other hand, SPIV (45°) shows less radial velocity downstream what was far away from physical understanding. Even though the averaged velocity in axial and radial component measured for PIV and SPIV (22.5°) show good agreement, it is still uncertain which SPIV set-up provides more accurate swirl components values. This component can not be evaluated just by these data here, further examination shall be done with those rms plotted in figure 12.

In figure 11 was found that the SPIV (22.5°) data set in axial and radial velocity agreed with PIV and provide reasonable values. The rms graphics show the same tendency for both components, with SPIV (22.5°) showing, in general, smaller rms than PIV. In the axial rms contour map, the fluctuation reaches its maximum values in the turbulent shear region, where the turbulent air-droplet mixing takes place. The swirl rms indicates that for SPIV (45°) the swirl velocity is measured with smaller fluctuation than for SPIV (22.5°). This fact, together with the smoothness of the swirl contours measured with 45° indicates that a bigger angle is more suitable for obtained this component. In figure 13, vorticity is plotted for the three cases, showing two big vortexes in the shear flow region

**Axial**

**Radial**

**Swirl**

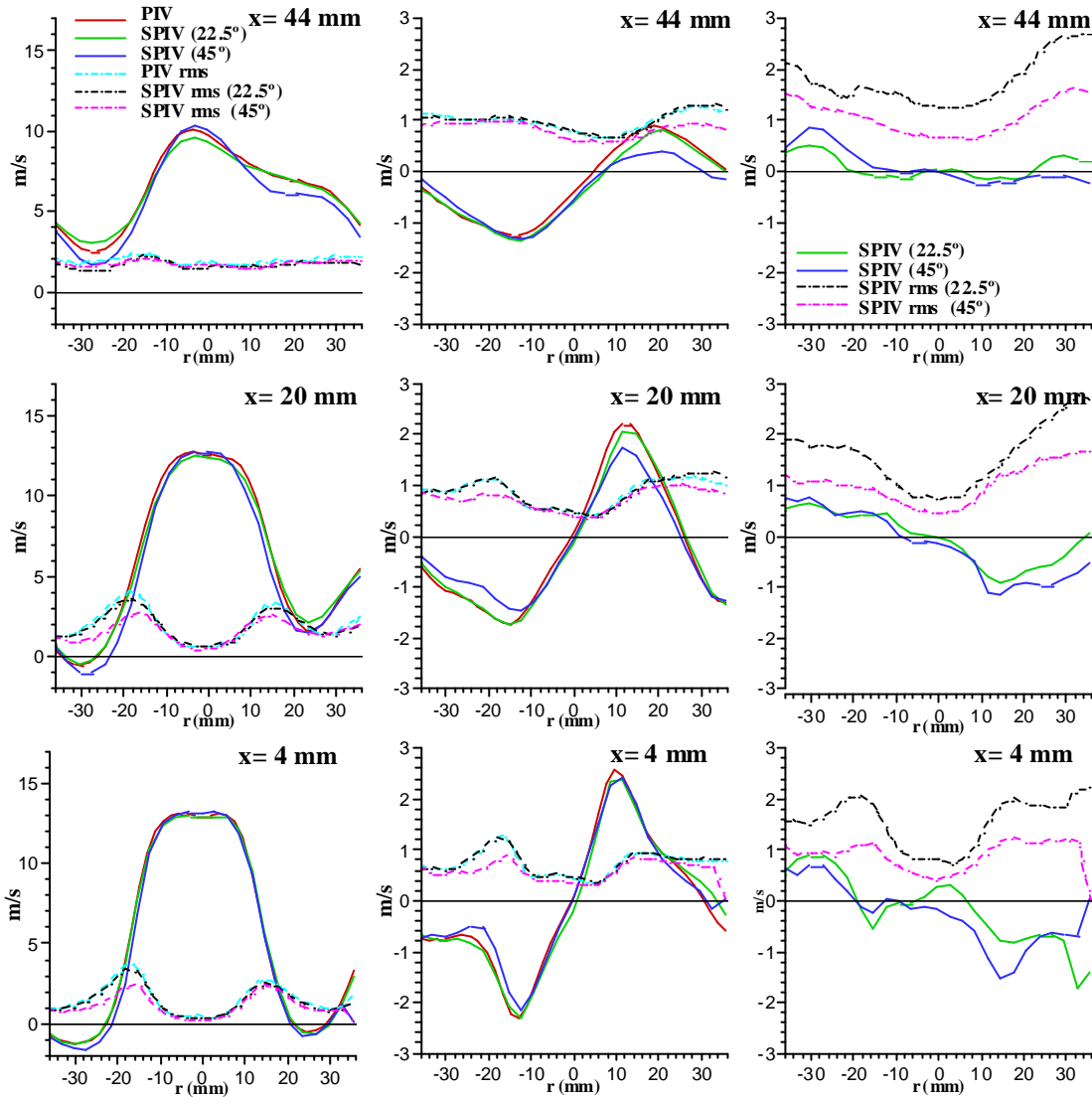


**Figure 14** Averaged SPIV and PIV velocity components at  $x = 4, 20$  and  $44$  mm

For a more detailed study, the velocity components values and their rms are plotted at different locations along the OX axis in figure 14. The first location ( $x = 4$  mm) corresponds to a line inside the recirculation zones. Maximum velocity in the axial component is near 13 m/s in the axis, and maximum velocity (in absolute value) in the recirculation zones is  $\sim 2$  m/s. The biggest difference in the velocity measured by PIV and SPIV is 1.33 m/s (10% of the maximum velocity) in the shear flow region. In the radial component, the maximum difference also corresponds to the left shear flow region ( $\sim 0.5$  m/s) while in swirl component the most important differences occurs near the spray axis, where the swirl component obtained with both angles has opposite direction. The rms of the three components shows two peaks located in the same position ( $r = 17$  mm,  $-17$  mm) but with different height. That indicates that the turbulence is affecting mainly the axial component measured with PIV (maximum rms  $\sim 3.5$  m/s) but its influence is not so strong in the other two components. In general, smaller fluctuations are obtained for SPIV ( $45^\circ$ ). The second location ( $x = 20$  mm) corresponds to the recirculation tail. For the axial and radial components the smallest difference between PIV and SPIV occurs near the central axis, and is maximum in both shear regions. For the swirl component the agreement between both profiles is evident. In the last location chosen upstream ( $x = 44$  mm), the axial and radial component lost its symmetry and the swirl component is almost zero, as expected. Now, the rms is almost constant for all radial positions as not significant process takes places at these locations.

## 5. CONCLUSION AND FUTURE WORK

Stereoscopic PIV has been evaluated in measurement of spatial spray characteristics, showing that is a reliable technique and can describe some important spray characteristics, such as the presence of the turbulent mixing zones, the presence of two recirculation zones and the influence of the baffle plate on the spray motion. Error estimation and optimization of optical set-up has been done to improve measurement and to estimate limitation of SPIV for spray research.

Axial and swirl data obtained by SPIV and PDA (SMD) has been compared, showing good agreement. For a more detailed analysis, SPIV has been compared with PDA size-classified data. PDA data were broken down into three classes: particles smaller than 30  $\mu\text{m}$ , between 30 and 50  $\mu\text{m}$  and bigger than 50  $\mu\text{m}$ . The best SPIV PDA agreement was found with sub-30  $\mu\text{m}$  particles, indicating that the SPIV settings used here were most capable of measuring this size class of particles.

PIV has been applied to this spray together with SPIV ( $2\alpha = 22.5^\circ$ ) and SPIV ( $45^\circ$ ). PIV and SPIV ( $22.5^\circ$ ) axial and radial component show a good agreement but for the swirl component better results are obtained with SPIV ( $45^\circ$ ). SPIV corrects the in-plane velocity components measured with PIV up to 10% of the maximum velocity value. Velocity fluctuation (rms) was also smaller for SPIV ( $45^\circ$ ) in the three velocity components.

Although the SPIV data appear to be more reliable than the PIV results, at this point one cannot say that they are ideal. Parameter optimization is needed and some parameters have been analysed in detail in a recent work (Palero et al 2000). It can, however, be said that combined with other techniques SPIV can provide a fuller understanding of the flow behavior. Future work will involve the application of Multi-intensity PIV with SPIV in order to describe droplet dynamics in the spray flame test rig.

## 6. REFERENCES

- Arroyo, M.P. and Greated, C.A., (1991), "Stereoscopic particle image velocimetry", *Meas. Sci. Technol.*, 2, 1181 – 1186.
- Bjorkquist, D.C., (1998), "Design and calibration of a stereoscopic PIV system", *Ninth. Symp. on Applic. of Laser Techniques to Fluid Mech.*, Lisbon.
- Gauthier, V. and Riethmuller, M.L., (1988), "Application of PIDV to complex flows: measurement of the third component", *KI Lecture Series on Particle Image Displacement Velocimetry* (Brussels).
- Grant, I., (1997), "Particle image velocimetry: a review", *Proc. Instn. Mech. Engrs.*, 211, part C, 55 – 76.
- Ikeda, Y., Kawahara N. and Nakajima T, (1995), "Flux measurements of  $\text{O}_2$ ,  $\text{CO}_2$  and  $\text{NO}$  in an oil furnace", *Meas. Sci. Technol.*, 6, pp. 826-832.
- Ikeda, Y., Yamada, N., Kawahara N., Shimo, D. and Nakajima T, (1998), "PIV application for spray characteristic measurement", *Ninth. Symp. on Applic. of Laser Techniques to Fluid Mech.*, Lisbon.
- Ikeda, Y., Yamada, N. and Nakajima T, (1999), "Spatial structure of a combusting spray by PIV", *First Int. Symposium of Turbulence and Shear Flow Phenomena*, Santa Barbara.
- Kawahara N., Ikeda, Y., Hirohata, T. and Nakajima T, (1996), "Size-classified droplets dynamics of combusting spray in 0.1 MW oil furnace", *Eighth. Symp. on Applic. of Laser Techniques to Fluid Mech.*, Lisbon.
- Kawahara N., Ikeda, Y., and Nakajima T, (1997), "Droplet dispersion and turbulent structure in a pressure-atomized spray flame", *AIAA*, paper 97-0125.
- Keane, R.D. and Adrian, R.J., (1990), "Optimization of particle image velocimeters, part I: double-pulsed systems", *Meas. Sci. Technol*, 1, pp. 1202-1215.

- Lawson, N.J. and Wu, J., (1997), "Three-dimensional particle image velocimetry: experimental error analysis of a digital angular stereoscopic system", *Meas. Sci. Technol.*, 8, 1455-1464.
- Palero, V., Andrés, N., Arroyo, M.P. and Quintanilla, M., (2000), "Holographic interferometry vs stereoscopic PIV for measuring out-of-plane fields in confined flows", *Meas. Sci. Technol.*, 11, 6, 655-666.
- Palero, V., Sato, K., Ikeda, Y., Nakajima, T and Shakal, J, "Stereoscopic particle image velocitmetry evaluation in a spray", Eight International Conference on Liquid Atomization and Spray Systems, Pasadena, US, 2000.
- Prasad, A.K. and Adrian, R.J., (1993), "Stereoscopic particle image velocimetry applied to liquid flows", *Exp. Fluids*, 15, 49 – 60.
- Prasad A.K. and Jensen, K., (1995), "Scheimpflug stereocamera for particle image velocimetry in liquid flows", *Appl. Opt.*, 34, 7092 – 7099.
- Raffel M., Willert, C and Kompenhans, J, (1998), "Particle image velocimetry- a practical guide", Springer-Verlag, Berlin Heilderberg.
- Yamada, N., Ikeda, Y., Nakajima, T., (1998), "Multi-intensity-layer PIV for spray measurement", Ninth. Symp. on Applic. of Laser Techniques to Fluid Mech., Lisbon.
- Willert, C., (1997), "Stereoscopic digital particle image velocimetry for application in wind tunnel flows", *Meas. Sci. Technol.*, 8, 1465-1479.